Volume 44   Issue 19   November 2010   ISSN 0043-1354

ELSEVIER

IWA **WATER RESEARCH**

A Journal of the International Water Association

Available at www.sciencedirect.com

ScienceDirect

journal homepage: www.elsevier.com/locate/watres
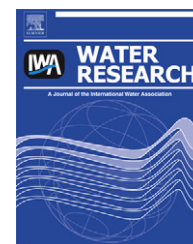
Fabrication and characterization of iron oxide ceramic membranes for arsenic removal

P. Sabbatini [a], F. Yrazu [a], F. Rossi [a,b], G. Thern [b], A. Marajofsky [b], M.M. Fidalgo de Cortalezzi [a,c,*]

[a] Centro de Ingeniería en Medio Ambiente, Departamento de Ingeniería Química, Instituto Tecnológico de Buenos Aires, Buenos Aires 1106, Argentina
[b] Comisión Nacional de Energía Atómica, San Martín, Argentina
[c] CONICET, Argentina

ARTICLE INFO

ABSTRACT

Nanoscale iron oxide particles were synthesized and deposited on porous alumina tubes to develop tubular ceramic adsorbers for the removal of arsenic, which is an extremely toxic contaminant even in very low concentrations. Its natural presence affects rural and low-income populations in developing countries in Latin America and around the world, which makes it essential to develop a user-friendly, low energy demanding and low cost treatment technology. The fabricated ceramic membranes can be operated with minimal trans-membrane pressure difference and do not require pumping. The support tubes and final membrane have been characterized by surface area and porosity measurements, permeability tests and scanning electron microscopy (SEM) imaging. Arsenic concentrations were determined by inductively coupled plasma–optical emission spectroscopy (ICP-OES). Due to its low cost and simple operation, the system can be applied as a point of use device for the treatment of arsenic contaminated groundwaters in developing countries.

1. Introduction

Arsenic contamination is a serious threat for human health and its incidence in the environment has been largely reviewed by the literature (Mandal and Suzuki, 2002; Smedley and Kinniburg, 2005). Arsenic is an abundant trace element and it exists in both inorganic and organic forms in water. It is present in the environment mainly in two oxidation states, arsenate and arsenite, the latter considered to be more toxic (Farquhar et al., 2002; Goldberg and Johnston, 2001). Arsenic mobilization occurs under natural conditions as a result of volcanic emissions, weathering reactions and biological activity. However, anthropogenic factors may have also contributed to magnify the problem. In fact, arsenic contamination has been increasingly reported in many countries around the world, such as Argentina, Chile, Mexico, USA, Canada, Spain, Greece, New Zealand, Japan, China, India, Vietnam, and the most critical case of Bangladesh in which 35–77 million people are at risk of drinking contaminated water (Mohan and Pittman, 2007; Smith et al., 2000). Argentina has possibly one of the largest areas with groundwater contamination (1 million square kilometers) with predominance of As(V) and concentrations up to 11,500 ppb for example in Cordoba province (Nicolli et al., 1989).

Chronic exposure to inorganic arsenic has been connected to skin, lung, bladder and kidney cancer as well as skin pigmentation and neurological disorders (Jain and Ali, 2000). The World Health Organization (WHO) has set the provisional guideline value of 0.01 mg/L (WHO, 2007) which has been adopted as a new standard in 2006 by the US-Environmental Protection Agency (EPA). However, several countries still maintain the previous WHO guideline of 50 ppb or are working on the technological aspects of conforming to lower regulations.

Many technologies have succeeded in removing arsenic from drinking water: coagulation/filtration, ion-exchange, membrane technologies, chemical precipitation and adsorption are the most relevant. A large fraction of the regions exposed to high arsenic concentration are developing countries with an important percentage of rural population. Consequently, there is a crucial need for specifically designed technologies for domestic water treatment systems. Unfortunately, most of the mentioned methods present disadvantages that make them unsuitable for small-scale applications as required by disperse populations situated in rural areas. For example, reverse osmosis membranes have a relatively high cost, and the need of electric power and technically skilled operators represents a disadvantage for isolated users. In the case of coagulation/filtration, its domestic application has the inconvenience of having to deal with sludge disposal, as well as the difficulty of achieving a complete separation of flocs. Ion-exchange and arsenic-specific adsorption media generally have relatively high costs for rural areas, and present availability and logistics constraints that make them mostly unsuitable for this type of application.

Adsorption is generally more attractive from the economical point of view than most other technologies reviewed. While activated carbon has been extensively used and reviewed as an adsorbent (Bansal and Goyal, 2005; Mohan and Pittman, 2007), it still remains rather expensive for developing countries. Therefore, other low cost adsorbents have been investigated such as activated alumina, hydrotalcites, oxides, phosphates and biosorbents; but the most promising and widely used are iron or iron compounds (iron oxides, oxyhydroxides and hydroxides) since they present higher adsorption capacity at a lower cost.

This study proposes the use of supported iron oxide ceramic membranes developed from iron oxide nanoparticles. The fabrication process starts from an iron oxyhydroxide (lepidocrocite, γ-FeOOH), whose particle size is reduced to nanoscale by reaction with an organic acid (in this case, acetic acid) (Rose et al., 2002). After this, the obtained particles are sintered to form an iron oxide (hematite) ultrafiltration ceramic membrane. Arsenic sorption onto hematite has been previously studied: Xu et al. (1988) described the inverse relation between pH and adsorption and Singh et al. (1996) found that the sorption could be fitted in a first-order kinetics model and Langmuir isotherm. Giménez et al. (2007) showed that natural hematite presents higher sorption capacity than natural magnetite and goethite, especially at acidic pH. There are no specific studies in the literature on sorption of arsenic onto hematite nanoparticles.

One advantage of our method lies in its economics: its manufacturing, operation and maintenance costs are convenient vis-à-vis other treatment methods. In addition to this, its compact and user-friendly design allows it to be deployed at the point of use, while it is also flexible to adapt to a larger scale, suitable for a municipal water treatment plant. Furthermore, the generation of liquid wastes on site can be avoided during operation, since arsenic is fixed in the solid phase. The membranes can be re-used after washing with a basic solution. The materials can be processed for regeneration in a centralized treatment facility for improved liquid waste management.

The objectives of this work are to (i) fabricate and characterize the ceramic membrane; (ii) obtain the adsorption isotherms and investigate the effects of pH, ionic strength and competitive ions and (iii) develop and analyze a potential operational scheme specifically tailored for domestic applications.

2. Materials and methods

2.1. Materials and chemicals

All chemicals were of reagent grade and solutions were prepared with water purified by reverse osmosis. Arsenic stock solutions were prepared using an arsenic standard solution (H_3AsO_4 in HNO_3 0.5 M, 1000 mg/L As; Merck, Darmstadt, Germany). Iron oxide nanoparticles were synthesized in the laboratory from industrial grade $FeCl_2$ (28–32% w/w; PPE Argentina S.A., Buenos Aires, Argentina). The synthesis takes place in two steps: (i) lepidocrocite and (ii) nanoparticles (ferroxanes) production. Lepidocrocite was obtained in the laboratory by pH controlled oxidation of ferrous chloride according to Schwertmann and Cornell (1991); afterwards, the lepidocrocite was centrifuged, washed and dried. Subsequently, the iron oxide was coated with acetic acid (Anedra, Buenos Aires, Argentina) to form carboxylate-FeOOH nanoparticles termed ferroxane-AA (Rose et al., 2002). These nanoparticles are precursors to ceramic membranes; they can be either deposited onto support matrices or dried to form a self-standing body. The nanoparticles are then sintered to form a porous hematite ceramic. Buffer solutions MES ($C_6H_{13}NO_4S$; Sigma, St. Louis, USA) and TRIS ($(HOCH_2)_3CNH_2$; Sigma, St. Louis, USA) were used to control pH. The electrolyte background was set with sodium nitrate ($NaNO_3$; JT Baker, Xalostoc, Mexico). All samples were acidified prior to arsenic measurement with ultrapure nitric acid (JT Baker, NJ, USA). The behavior of adsorption in the presence of competitive ions was studied by adding NaF (Anedra, Buenos Aires, Argentina) and $SiO_2 \cdot H_2O$ (Riedel-de Haën, Germany).

2.2. Characterization of iron oxide nanoparticles

The behavior of the iron oxide nanoparticles at different temperatures was initially investigated by Thermal Gravimetric Analysis (TGA) performed up to 450 °C with a setup built in the laboratory consisting of an analytical balance (A&D, Japan; readability. 0.1 mg and RS-232 communication port) inside a digitally controlled furnace. In addition to this, the following analyses were conducted to five samples fired at different sintering temperatures (250, 300, 350, 400 and

450 °C): powder X-ray diffraction (XRD) was conducted using a PW 1730/10 X-ray diffractometer (Philips, Netherlands) using Cu Kα radiation (tension = 40 kV, current = 20 mA); the surface morphology was studied by scanning electron microscopy (SEM) using a Philips XL30 TMP (Philips, Netherlands) microscope; the specific surface area was measured by Brunauer–Emmett–Teller (BET) N_2 method and the pore size was calculated by the Barrett, Joyner and Halenda (BJH) N_2 adsorption/desorption isotherm method at 77 K using the Coulter™ SA 3100™ (Beckman Coulter, USA) analyzer. The synthesis process was studied by characterizing the intermediate products. XRD was performed to the prepared lepidocrocite and unsintered ferroxanes-AA while surface area and pore size distribution analyses were carried out to sintered ferroxanes. Additionally, the particle size of unsintered ferroxanes-AA was measured by using a Zetasizer Nano (Malvern, UK) particle analyzer to study the influence of stirring and sonication over time.

2.3. Adsorption isotherms

Batch experiments were conducted at room temperature adding a constant mass of iron oxide (0.5 g/L) to a solution of changing initial As(V) concentration (1–10 ppm). The objective was to study the adsorption isotherms under the influence of pH (pH 3.0, 6.1 and 8.0), ionic strength (IS) (1, 10 and 100 mM) and in the presence of competitive ions (F^- and SiO_2). The background electrolyte was $NaNO_3$. The levels of competitive ions (1 ppm F^- and 20 ppm SiO_2) were set following the National Science Foundation (NSF) challenge
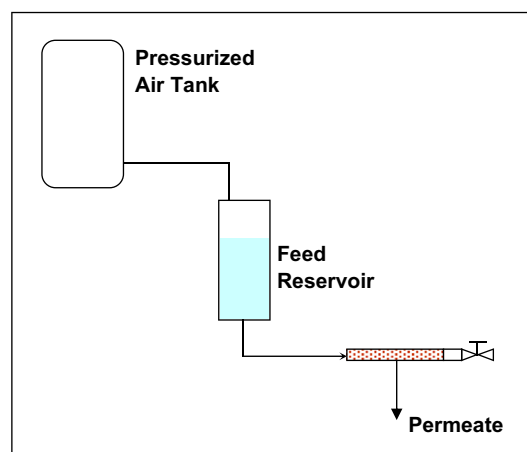
Fig. 1 – Operational setup.

water standards. The pH value was controlled throughout the experiments. MES buffer was used to set the reference case pH in 6.1 since it is representative of most groundwaters. For the pH 8.0 samples Tris buffer was employed. After 48 h, samples were centrifuged and filtered using a 0.22 μm filter. Before analyzing, all samples were preserved for arsenic analysis by acidifying them with 0.3% of HNO_3. The arsenic content in the supernatant solution was then analyzed by ICP-OES (detection limit 5 ppb). The adsorption capacities were calculated from the difference between the initial and the equilibrium concentrations.

Fig. 2 – SEM images of iron oxides sintered at (a) 250 °C, (b) 300 °C, (c) 350 °C and (d) 450 °C.

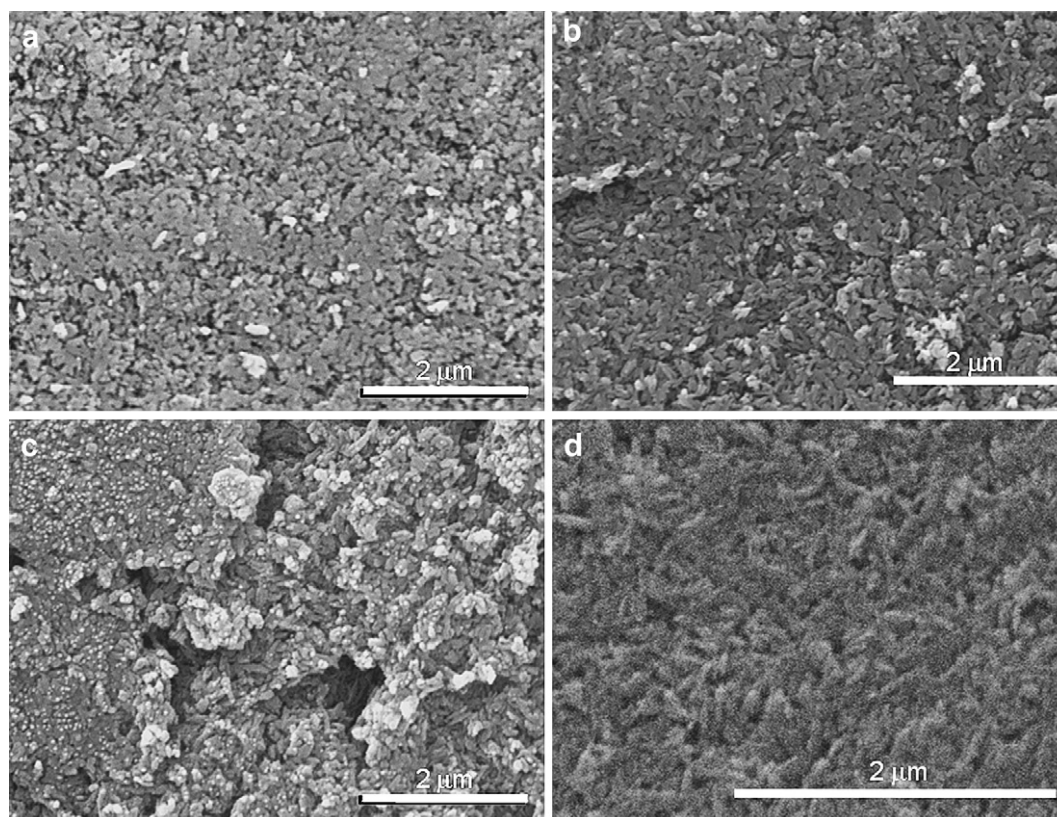| Table 1 — Characterization of the iron oxide nanoparticles synthesis process.									
Batch number	Batch #	Yield	Particle size		Yield	Sintered iron oxide			
						Surface area	Average pore size		Yield
		g Lep/g FeCl$_2$	Avg. (nm)	Std. Dev. (nm)	g Fe$_2$O$_3$ (u)/g Lep	Avg. (m^2/g)	Avg. (nm)	Std. Dev. (nm)	g Fe$_2$O$_3$ (s)/g FeCl$_2$
L0608	1	22%	288.02	3.15	50%	47.016	62.35	34.29	8%
L1008	2	25%	251.57	48.25	52%	46.026	76.00	39.40	10%
L1108	3	18%	191.86	17.41	66%	37.985	80.85	38.38	9%
L1208	4	32%	n/d	n/d	24%	34.479	61.87	35.09	6%
L1308	5	34%	n/d	n/d	27%	43.891	61.31	40.80	7%
Average		26%	243.81		44%	41.879	68.48		8%
Std dev.		7%	48.54		18%	5.421	9.25		2%
(u): unsintered; (s): sintered.									

2.4. Operational setup

It consisted of an alumina-supported iron oxide ceramic tube with a dead end. This type of membrane was fabricated by depositing the iron oxide particles onto the alumina supports. A suspension of these nanoparticles was filtered inside-out through the support tubes with one end closed so that all the water was forced through the ceramic, while the iron oxide particles were retained. The filter was then dried and sintered. For treatment of As containing solutions, a filtration cell containing the feed solution was connected to the iron oxide-loaded tube which had the other end closed (Fig. 1). Air was supplied to the filtration cell at 0.5 bar to drive the arsenic solution through the inner hole of the tube, forcing the permeate to flow radially through the tube with the iron oxide nanoparticles deposited on the alumina. The permeate was sampled and tested for arsenic. The tubes were 100—150 mm long and 5—8 mm thick. In order to characterize the alumina ceramic supporting tubes permeability tests were carried out filtering pure water at constant pressure through the untreated tube.

2.5. Membrane regeneration

The membrane was treated with NaOH at pH 11 with the aim of recovering its adsorption capacity, based on the fact that at high pH the anion desorption is favored. After the basic
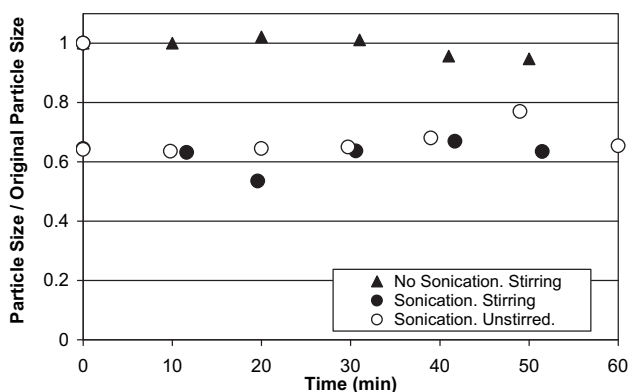
treatment the tube was rinsed with deionized (DI) water. The washing solution exiting the membrane was sampled and analyzed for arsenic.

3. Results and discussion

3.1. Characterization of iron oxide nanoparticles and ceramic material (see supporting information in Appendix A)

XRD was performed in order to determine the lowest sintering temperature at which full conversion of ferroxane nanoparticles into the stable phase (hematite) was achieved, minimizing the loss of specific surface area due to thermal-induced densification. Maghemite is the primary phase observed between 250 °C and 300 °C (Schwertmann and Cornell, 2000). The XRD analysis revealed that 350 °C is the optimal sintering temperature since it is the lowest temperature at which the material undergoes practically complete conversion to hematite (96.9% hematite, 3.1% maghemite), while the particles are successfully bonded to the support (Figure A.1, Appendix A). Therefore all iron oxide nanoparticles used in the experiments, both supported and unsupported, were sintered at 350 °C.

The TGA performed on carboxylate-FeOOH nanoparticles showed that the most evident weight loss occurs first at 100 °C and later at 200—250 °C, probably due to the evaporation of water and organic compounds (Figure A.2, Appendix A). However, after 300 °C no further significant mass loss occurs. In total 25% of the mass is lost within the sintering process.

The results of the area analyses (Figure A.3, Appendix A) at different sintering temperatures indicate that, as was expected, the surface area decreases with increasing temperature, ranging from 74 m^2/g at 250 °C to 30 m^2/g at 350 °C. The slope then flattens with only a slight change up to 450 °C. The average pore size rises slightly with temperature (75 nm at 350 °C).

Images of the surface morphology of samples at temperatures between 250 °C and 450 °C (Fig. 2) do not exhibit significant changes, as higher temperature samples retain the characteristic surface roughness of this material. While in the low temperature images (a, b) individual particles can be identified, the higher temperature images (d) show slightly bigger features due to ceramic densification.

Fig. 3 — Influence of stirring and sonication in particle size over time.
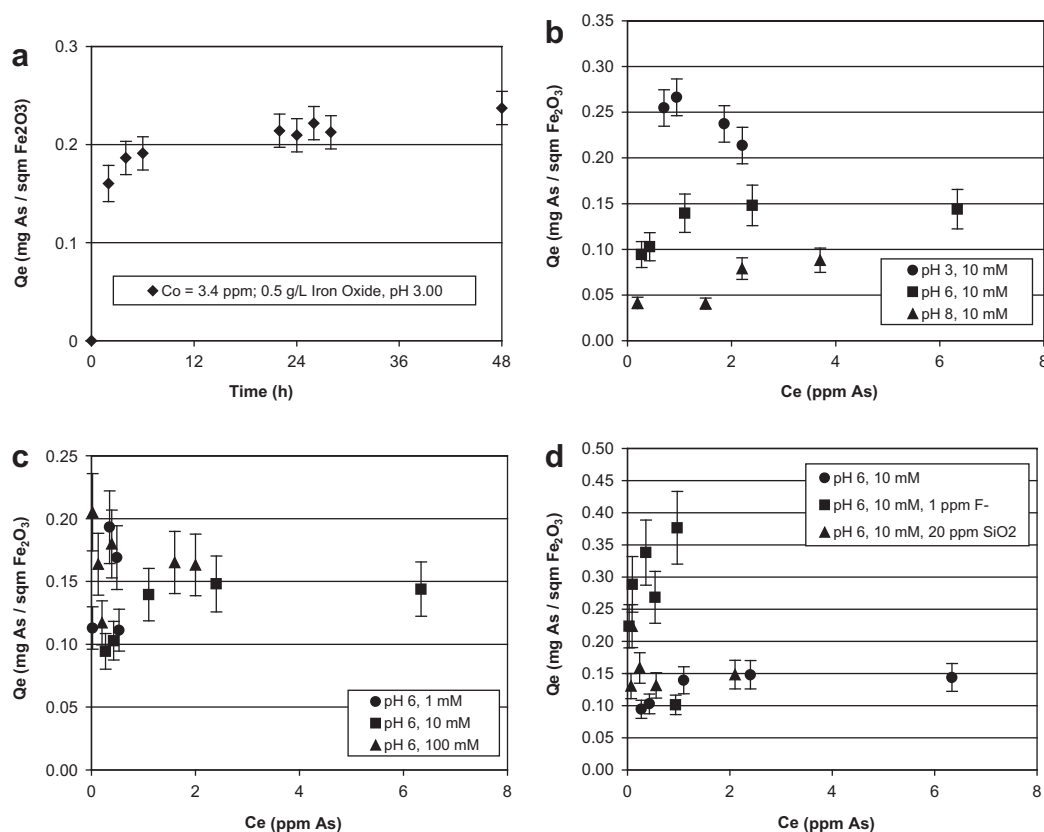
Fig. 4 – (a) Kinetics of As(V) sorption (3.4 ppm, 0.5 g/L of iron oxide and pH 3.00), (b) adsorption isotherms of pH 3.0, 6.1 and 8.1; (c) adsorption isotherms of IS 1 mM, 10 mM and 100 mM and (d) adsorption isotherms of competitive ions F^- and SiO_2.

Once the sintering temperature was determined to be 350 °C, the five batches of iron oxide nanoparticles employed to carry out this study were characterized. XRD, particle size, surface area (Table 1) and pore size distribution analyses were performed throughout the manufacturing process. The average pore size of the sintered iron oxide is 68.48 ± 9.25 nm and the average surface area (41.879 ± 5.421 m²/g). The total yield of the manufacturing process (8% g Fe_2O_3/g $FeCl_2$) remains relatively low and the limiting step seems to be the synthesis of the lepidocrocite. In fact, Schwertmann and Cornell (1991) inform a typical conversion of 50% g lepidocrocite/g $FeCl_2$. This yield may be lower due to the use of industrial $FeCl_2$, in addition to the many variables that must be controlled during the process and which can potentially have an effect on the outcome. For example, correct regulation of pH during the initial part of the lepidocrocite manufacturing process, as well as adequate stirring to ensure

homogeneity and sufficient aeration. These kinds of variation, and also that of the resulting surface area, are within the expected range for a multistage process and the inherent variability of the BET determination. Even so, the cost remains negligible in comparison with the reagent grade ferrous chloride.

In order to obtain uniform deposition of the iron oxide nanoparticles into the alumina supporting tubes, it was necessary to determine whether stirring or sonication had any influence on particle aggregation. In fact, aggregates in the precursor solution previous to deposition will result in a heterogeneously coated support, probably leading to a low efficiency in the treatment due to hydraulic shortcuts and areas of high hydraulic resistance. Three cases were tested: stirring without previous sonication, sonication without stirring, and sonication with stirring (Fig. 3). While only stirring the sample does not have a significant effect on particle size,

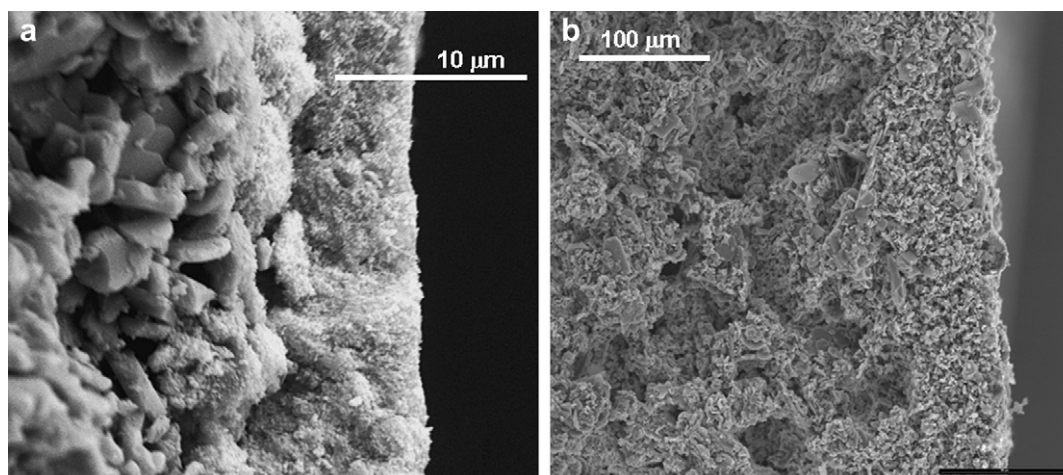| Table 2 – Conditions of batch adsorption isotherms experiments.								
		Acid pH	Base case	Basic pH	Low IS	High IS	$+F^-$	$+SIO_2$
$NaNO_3$	mM	10	10	10	1	100	10	10
MES buffer	mM	0	5	0	5	5	5	5
TRIS buffer	mM	0	0	5	0	0	0	0
IS	mM	12–13	14–18	12–14	5–6	105–106	14–16	15–16
pH	–	2.98–3.08	6.02–6.20	7.86–8.04	6.15–6.27	6.1–6.27	6.07–6.36	6.10–6.28

Fig. 5 – SEM images showing (a) the deposit of iron oxides on the inner surface of sample A tube and (b) sample B tube with the external layer.

sonication reduces it to 60% of its initial value. Further stirring after sonicating does not seem to keep contributing to the disaggregation process. Therefore, before coating the alumina tubes, the iron oxide particles were sonicated for 5 min to improve the supported filter quality.

3.2. Adsorption isotherms

The kinetic experiment in Fig. 4a was performed to determine the time for equilibrium in batch experiments. After 48 h, a flattening of the slope in the adsorption of arsenic onto the solid was observed (pH 3; 0.24 mg As/m^2 Fe$_2$O$_3$). Therefore, all batch experiments were stirred for two days to determine the equilibrium data.

The adsorption isotherms of arsenate onto ferroxane-derived hematite were obtained under different relevant conditions. Based on the data from the base case (pH 6.1; IS 10 mM), the adsorption of arsenate onto hematite may be described by a Langmuir type isotherm in which adsorption is limited by surface saturation. The Q coefficient [mg As/m^2 iron oxide] represents the adsorption capacity of the ceramic, while the b coefficient [L/mg As] is called the Langmuir constant and is related to the affinity of the adsorbent for the solute (Eq. (1)). In this case, we obtained a good Langmuir fit ($R^2 = 0.955$), with $Q = 0.154$ mg As/m^2 iron oxide, and $b = 5.52$ L/mg As.

Several researchers have also suggested a Langmuirian type adsorption of arsenite and arsenate on iron oxides (Ferguson and Davis, 1972; Holm et al., 1979). However, no good fit could be obtained for other conditions. This was caused in part by the difficulty to obtain data points due to iron dissolution, the inherent variability of the adsorbent material, and the limitations of the analytical methods employed.

The base case was compared according to pH variation, ionic strength variation and the presence of competitive ions. Table 2 summarizes the conditions in which the seven experiments were performed.

It was confirmed that adsorption decreases with the rise of pH (Fig. 4b), which is consistent with the literature on the subject (Schwertmann and Cornell, 2000). In this dominant specific adsorption mechanism, arsenate replaces the surface hydroxyl groups. Increasing pH causes the decrease of surface FeOH$^+_2$ groups, inhibiting the sorption. This sharp variation in the adsorption capacity of the membrane is one of the key aspects of its regeneration capability. Indeed, the adsorption capacity at pH 8 is at least 40% less than that at pH 6, which explains the fact that flushing the membrane with a basic solution desorbs a large percentage of the arsenic that had been originally retained.

The high ionic strength isotherm (100 mM, 0.16 mg/m^2) does not appear to be significantly different from the base case (10 mM, 0.145 mg/m^2) (Fig. 4c). In the low ionic strength experiment (1 mM) samples with an initial adsorbate/adsorbent ratio above 7 mg As/g Fe$_2$O$_3$ suffered iron dissolution, so it was not possible to obtain reliable data. Nevertheless, the data points indicate a similar adsorption behavior compared to the base case. These results are consistent with specific adsorption mechanisms, in which electrostatic interactions (regulated by the ionic strength of the solvent) are not the determinant mechanism for attachment of the adsorbate. This is in agreement with the literature regarding the adsorption of arsenate anions onto iron oxides, which shows greater adsorption for arsenate at lower pH (Pierce and Moore, 1982).

Table 3 – Permeability of both types of alumina ceramic tubes before and after being coated with Fe$_2$O$_3$ and sintered.

Sample	Permeability (L h^{-1} m^{-2} bar^{-1})	
	Untreated	Treated[a]
Type A tube	916 ± 251	575 ± 309
Type B tube	9777 ± 571	2935 ± 579

a Sintered with Fe$_2$O$_3$.

Many authors have studied the effect of competitive ions, such as fluoride or silica, on arsenic adsorption (Möller and Sylvester, 2008). With the rise of polymeric silica at higher pH levels, the surface of the iron oxides tends to be coated by the silica species and the electrostatic repulsion of arsenic anions is increased. However, at pH 6.1 (which is representative of most groundwaters) the decrease in the adsorption capacity was not noticeable. In a similar way, the presence of fluoride anions did not hamper the adsorption of arsenic (Fig. 4d). The results might hint at a collaborative effect, although further studies are required. In the light of their experiments with a similar material (Ce-doped iron oxides), Zhang et al. (2003) suggested that the adsorption sites for As and F⁻ are not the same. This is a very important fact for the correct functioning of the membrane, given that usually fluoride is concomitantly found in waters with high arsenic levels.

3.3. Operational scheme: alumina-supported iron oxide ceramic tube

Before fabricating the supported membrane, the alumina ceramics proposed as support material were characterized. Several support pore sizes were studied. It was observed that those tubes with an average porosity of order 1 micron (type A) caused the iron oxide particles to deposit on its inner surface, possibly due to aggregates in solution. In this case, a very thin layer of iron oxide was formed on the inside of the tubes

(Fig. 5a) and the trans-membrane pressure drop increased significantly for the asymmetric ceramic membrane obtained due to the relatively small pore size of this layer that caused the particles to be retained completely by the support material. Fig. 5a also presents the difference between the shape of the Fe$_2$O$_3$ and Al$_2$O$_3$ particles. The iron oxide particles are clustered and aggregated while the alumina particles present an acicular shape with a smooth surface. To prevent the complete retention of the particles on the surface of the support, a more porous type of alumina tube (type B, 20–60 microns) was coated on the outer side with a smaller pore size alumina (1 micron) shown in Fig. 5b. In this way, particles easily entered the highly porous section of the supports and were then effectively retained by the outer layer. The cake formed inside type A tubes prevented further particle deposition inside the tube while type B tubes allowed the particles to deposit from the outer to the inner region of the tube. Therefore, the already deposited particles acted as the external layer to the next deposited particles which resulted in a more advantageous use of the support material.

The characterization of both samples included permeability tests. Clean water filtrations were performed with both tube types and the permeate flow was measured before and after being charged with the iron oxide nanoparticles and being sintered. Table 3 presents the permeability results of type A and type B tubes. After the treatment process, it is observed that type B permeability decreases twice as much as
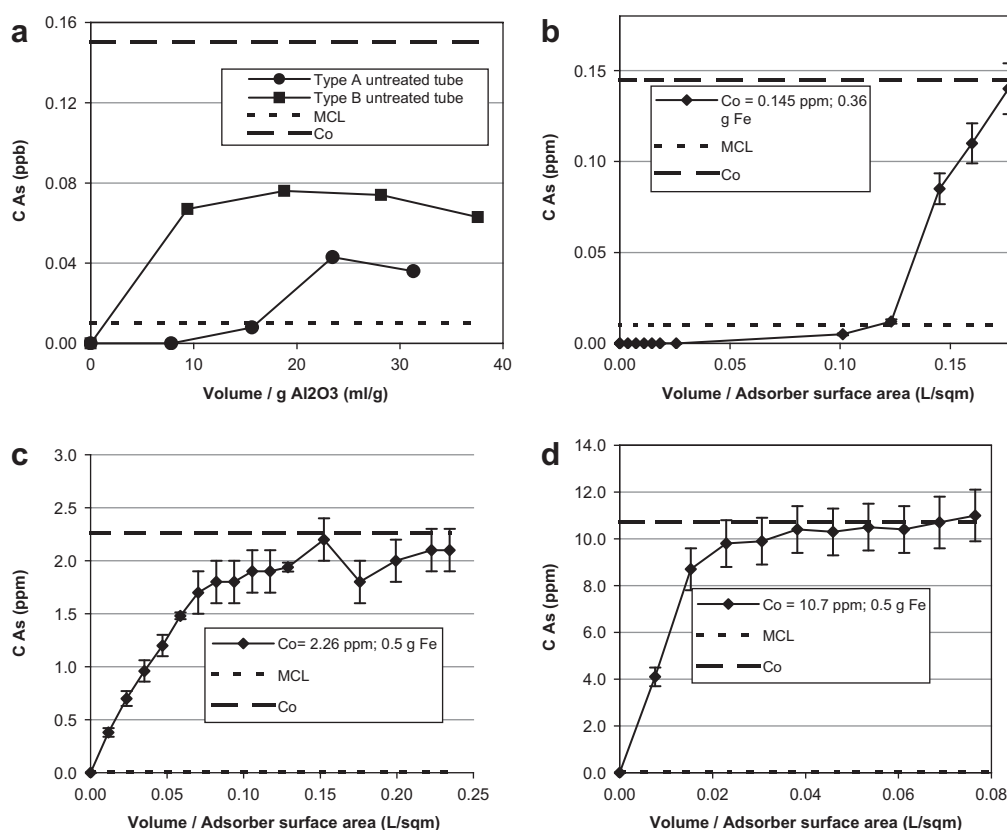
Fig. 6 – (a) Breakthrough curve of alumina sample A and sample B tubes (initial concentration: 150 ppb, pressure: 0.5 bar, flow rate: 2.8 L/h); Breakthrough curves of the supported membrane setup: (b) Natural water from the city of 9 de Julio (see Table B.1, Appendix B). Initial concentration (Co): 0.145 ppm, ΔP: 0.4 bar, flow rate (Q): 0.4 L/h, pH: 6.1; (c) Lab-prepared As solution. Co: 2.26 ppm, ΔP: 0.4 bar, Q: 0.82 L/h, pH: 6.45; (d) Lab-prepared As solution. Co: 10.7 ppm, ΔP: 0.5 bar, Q: 1 L/h, pH: 6.45.

Table 4 – Iron-based adsorbents for drinking water and their adsorption capacities.

Adsorbent	pH	Concentration/range	Surface area (m²/g)	T (°C)	Method	Capacity (mg/g) As(V)	Ref
Unsupported material							
Akaganeite β-FeO(OH) nanocrystals	7.5	5–20 mg/L	330	25	Langmuir	141.3	Solozhenkin et al. (2003)
FePO₄ (amorphous)	6–6.7	0.5–100 mg/L	53.6	20	–	10	Lenoble et al. (2005)
FePO₄ (crystalline)	6–6.7	0.5–100 mg/L	35.9	20	–	9	Lenoble et al. (2005)
Ferrihydrite	7	0–150 mg/L	–	–	Langmuir	68.75	Lafferty and Loeppert (2005)
Ferrihydrite	–	0.267–26.7 mmol/L	–	–	–	111.02	Raven et al. (1998)
Fex(OH)y-Montm	9	0–60 mg/L	165	22	–	4	Lenoble et al. (2002)
Goethite	9	0–60 mg/L	39	22	–	4	Lenoble et al. (2002)
Goethite	5	–	103	29	Langmuir	5	Lakshmipathiraj et al. (2006)
Goethite	7.1	0–38 mg/L	–	–	Langmuir	442.8	Lafferty and Loeppert (2005)
Hematite	4.2	133.49 mmol/L	14.4	30	Langmuir	0.2	Singh et al. (1996)
HFO	9	0–60 mg/L	200	22	–	7	Lenoble et al. (2002)
Small SORB 33, Severn Trent company	6.8	0.02 mg/L	–	–	–	6.22	Kumar et al. (2008)
Nanostructured akaganeite	7.5	5–20 mg/L	330	25	Langmuir	1.8	Deliyanni et al. (2003)
Supported material							
This Study	6.1	2–10 mg/L	41.879	25	*Langmuir*	5.99	–
	6.1	10 mg/L	26.149	25	*Breakthrough*	4.35	–
	6.1	0.145 mg/L	37.985	25	*Breakthrough*	0.79	–
Alginate bead (doped and coated with iron)	7	50 µg/L	–	25	Column capacity	0.014	Zouboulis and Katsoyiannis (2002)
Alumina/Fe(OH)₃	8.2–8.9	0.05 mg/L	–	–	Breakthrough	0.09	Hódi et al. (1995)
Fe/NN-MCM-41	6	0–1500 mg/L	310	25	–	119.8	Yoshitake et al. (2003)
Fe/NN-MCM-48	6	0–1500 mg/L	352	25	–	187.3	Yoshitake et al. (2003)
Fe10SBA-15	6.5	0.133–1.33 mmol/L	–	25	Langmuir	12.74	Jang et al. (2003)
Ferric chloride impregnated silica gel	–	–	–	–	–	≤5.24	Isao et al. (1976)
GAC-Fe (0.05 M)	4.7	0.10–30.0 mg/L	600–1000	25	Langmuir	2.96	Gu et al. (2005)
GAC-Fe–H₂O₂ (0.05 M)	4.7	0.10–30.0 mg/L	600–1000	25	Langmuir	3.94	Gu et al. (2005)
GAC-Fe–NaClO (0.05 M)	4.7	0.10–30.0 mg/L	600–1000	25	Langmuir	6.57	Gu et al. (2005)
GAC-Fe–O₂ (0.05 M)	4.7	0.10–30.0 mg/L	600–1000	25	Langmuir	1.92	Gu et al. (2005)
Granular ferric hydroxide (GfH)	8–9	5–100 mg/L	–	25	Column capacity	2.3	Catalano et al. (2007)
Iron hydroxide coated alumina	7.15–7.2	0.1–1.8 mmol/L	95.7	25	Langmuir	36.64	Hlavay and Polyák (2005)
Iron oxide coated cement (IOCC)	7	0.5–10.0 mg/L	–	35	Langmuir	6.43	Kundu and Gupta (2006)
Iron oxide coated sand	7.6	100 µg/L	10.6	22±2	Langmuir	0.043	Thirunavukkarasu et al. (2003)
Iron(III) alginate gel	4	0–10 mg/L	–	–	–	352	Min and Hering (1998)
Iron(III) oxide with polyacrylamide	–	–	–	–	–	43	Shigetomi et al. (1980)
Iron(III) oxide-impregnated GAC	7	1 mg/L	840	20–23	–	4.5	Reed et al. (2000)
Iron(III)-loaded chelating resin	–	–	–	–	–	60	Rau et al. (2000)
Sulfate-modified iron oxide coated sand (SMIOCS)	7	0.5–3.5 mg/L	3.75	27	Langmuir	0.12	Vaishya and Gupta (2004)
Sulfate-modified iron oxide coated sand (SMIOCS)	4	0.5–3.5 mg/L	3.74	27	Langmuir	0.13	Vaishya and Gupta (2004)

type A permeability. Nevertheless, sintered tube B still remains 5 times more permeable than the sintered type A sample. As a result, type B was chosen as the support alumina material for the fabrication of the iron oxide membranes. The decrease in permeability is explained by the densification of the particles after the sintering process and the decrease in the pore volume due to the deposition of the iron oxide nanoparticles.

To identify whether alumina favored significantly the adsorption of arsenic, the same solution (1.5 ppm As(V)) was filtered through both untreated tubes (Fig. 6a). The adsorptive capacity of both tubes was not significantly different. The alumina contribution to the adsorption is $(3.7 \pm 0.6) \times 10^{-3}$ mg As/g Al$_2$O$_3$ which indicates that the iron oxide is the primary material for the adsorption.

Fig. 6d presents the results obtained from the supported membrane experiment. In this case a single type A tube (26 g, 76 mm long, 8 mm thick, diameter 13 mm) was charged with 0.5 g of previously sonicated iron oxides and then sintered at 450 °C (26.149 m^2/g). In order to assess its adsorption capacity, 400 mL of a 10 ppm arsenic solution were filtered at a constant pressure of 0.5 bar and 50 mL samples were taken every 100 mL. After 400 mL, the arsenic concentration in the permeate reached the initial concentration, which indicated that no further significant adsorption was taking place. Consequently, the calculated adsorption capacity is 0.166 mg As/m^2 Fe$_2$O$_3$.

This experiment was repeated with another type A tube charged with approximately 0.1 g of iron oxide and an initial concentration of 2.26 ppm. After a volume of 2000 mL was filtered, the permeate As concentration reached initial levels (Fig. 6c). The adsorption capacity for this case was determined to be 0.144 mg As/m^2 Fe$_2$O$_3$.

A similar experiment was conducted with another type A tube charged with 0.36 g of iron oxide and an initial concentration of 0.145 ppm (Fig. 6b). In this case saturation was reached after filtering 2300 mL of solution, giving an adsorption capacity of 0.021 mg As/m^2 Fe$_2$O$_3$. After 1600 mL were filtered, the maximum contaminant level (MCL: 10 ppb) was exceeded.

The adsorption capacity depends on the adsorbate/adsorbent ratio (Pierce and Moore, 1982). Observations suggest the higher the As(V) concentration per mass of iron oxide, the higher the adsorption. This could be partially explained by the fact that the stronger driving force, created by a higher concentration gradient between the pore volume inside the particles and the bulk solution, helped the diffusion step and therefore resulted in a different pseudo-equilibrium state.

The batch experiments provided an estimate of the material adsorption capacity of 0.145 mg As/m^2 iron oxide. The filtration experiments gave a saturation As concentration in the solid of 0.022 mg As/m^2, 0.144 mg As/m^2, and 0.166 mg As/m^2 for an incoming arsenic solution of 0.145 ppm, 2.26 ppm and 10.7 ppm, respectively. These adsorption capacities are in good agreement with the predicted values based on the corresponding adsorption isotherms (pH = 6) for those equilibrium concentration levels.

Despite the fact that batch and breakthrough experiments exhibited similar adsorption capacities, it should be pointed out that in the batch setting, it takes several hours to reach the equilibrium concentration (Fig. 4a), while for the filtration

breakthrough experiments, it does so in a matter of minutes (that is, in a time lapse equal to the residence time). In the batch experiments, as-prepared iron oxide ceramic (unsupported) was broken into approximately 1 mm particles and stirred in the arsenic solution. While part of the area is readily available for the ions to adsorb, there is an important inner surface area where the arsenate ion can only access by diffusion within the porous structure, making it the limiting step in the adsorption process. This is consistent with other reports that show two different diffusive stages in anion adsorption: a first rapid one in which diffusion occurs mainly in readily accessible sites and a second slower one in which the adsorbing species diffuse into particle aggregates; crystal micropores are rearranged into surface complexes (Schwertmann and Cornell, 2000). In fact, filtration may turn previously slow stage sites into readily accessible ones, enhancing the rapid initial stage of the adsorption process compared with the batch operational scheme.

Mohan and Pittman compared the adsorption capacities of various adsorbents for arsenic removal (Mohan and Pittman, 2007). Table 4 summarizes the capacity of As(V) removal of iron-based adsorbents in drinking water. The adsorption capacity results from this work are comparable to other technologies with similar surface area values. In addition, while other adsorbents present smaller particles with higher adsorption capacities, they are usually related to higher energy-associated manufacturing costs.

Based on the fact that specific adsorption is the dominating mechanism and that at high pH levels there is a drop in the number of adsorption sites, the anion desorption is favored; therefore the membrane was treated with pH 11 solutions to regenerate the adsorption capacity. Regeneration efficiency was calculated as the ratio of mass of arsenic present in the used washing solution to the mass retained during each treatment cycle. The efficiency (Eq. (2)) decays from 60% to 12% throughout 6 regenerating cycles, which may suggest some degree of irreversibility in the desorption process (Fig. 7). However, since the arsenic concentrations found in the permeate were too close or even below the detection limit of the measuring instrument, the experimental error in the calculated mass balances diminished the accuracy of the
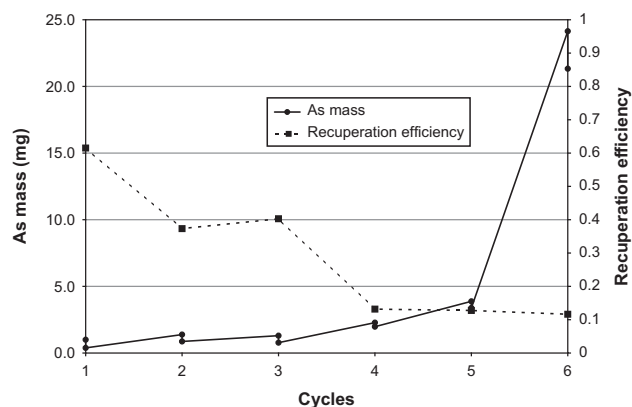

Fig. 7 – Arsenic recuperation efficiency after repeated filtration–wash cycles; the calculated mass of arsenic present in the filter previous to each wash cycle is indicated on the left y-axis.

obtained efficiency values. The membrane remained intact during over 6 adsorption–desorption cycles, since no iron dissolution was detected during the basic washes.

4.　　Conclusions

Supported and unsupported iron oxide ceramic membranes were fabricated and successfully applied to the removal of arsenic from drinking water

- The optimal sintering temperature in which the ferroxanes-AA are fully transformed into hematite is 350 °C. At this temperature, the average surface area is 41.879 ± 5.421 m^2/g and the average pore size is 68.48 ± 9.25 nm.
- TGA analysis revealed that 25% of the total mass is lost during the sintering process. The total yield of the manufacturing process is 8% which is still relatively low. Consequently, alternatives to increase this efficiency are being investigated.
- Adsorption is enhanced in acidic conditions, but is not significantly altered by ionic strength variations, which suggests a predominant specific adsorption mechanism. Moreover, the concentration of SiO_2 and F^- used in the experiments did not show intereference effects.
- The reference batch isotherm (pH 6.10, 10 mM IS) revealed an adsorption capacity of 0.145 mg/m^2.
- Breakthrough experiments were performed with the alumina-supported iron oxide ceramic tube and resulted in adsorption capacities of 0.166 mg As/m^2 Fe_2O_3 (10 ppm), 0.144 mg As/m^2 Fe_2O_3 (2.26 ppm) and 0.021 mg As/m^2 Fe_2O_3 (145 ppb). Compared with the batch results, the filtration setup appears to increase the adsorption reaction progression rate, reaching near-equilibrium in a much shorter time.
- The regeneration process was applied during up to 6 cycles, removing the As(V) present in the membrane without dissolving iron.
- This material's adsorption capacity is acceptable vis-à-vis other adsorbents with a comparable surface area.
- The cost of the unsupported hematite ceramic nanoparticles is estimated to be around 24 USD/kg, although these costs would almost surely be significantly reduced when transitioning from laboratory scale to pilot plant or industrial production.
- In the case of the alumina-supported membranes, estimating a 10-g hematite load per tube, the cost of the iron oxide turns to be almost negligible (approximately 25 cents) when compared to the cost of the support itself (approximately 12 USD per tube). However, it should be taken into account that these tubes are expected to withstand several regeneration cycles, which keeps them cost-competitive when compared to single-use technologies. Substantial cost reductions are expected with larger scale production. In addition to this, ferroxane-derived ceramic membranes have removal capabilities in the ultrafiltration range, being effective for the separation of organic macromolecules, inorganic colloidal particles and bacteria (Cortalezzi et al., 2003). Current research aims at investigating the removal capacity for viral contamination (Attinti et al., 2010), further increasing the value of the material through multiple functionalities.

Appendix.

$$\frac{1}{Qe} = \frac{1}{Q \times b} \times \frac{1}{Ce} + \frac{1}{Q} \tag{1}$$

Equation 1 – Langmuir linearization. Qe [mg As/m$_2$ iron oxide] is the equilibrium adsorption capacity of the iron oxide for a given equilibrium concentration of arsenic in solution Ce [mg As/L]. The Q coefficient [mg As/m^2 iron oxide] represents the adsorption capacity of the ceramic, while the b coefficient [L/mg As] is called the Langmuir constant and is related to the affinity of the adsorbent for the solute.

$$r_e = \frac{\sum C_{i,\text{wash}} \times V_{i,\text{wash}}}{C_{\text{in}} \times V_{\text{in}} + As_{\text{orig}} - \sum \left(C_{j,\text{permeate}} \times V_{j,\text{permeate}} \right)} \times 100\% \tag{2}$$

Equation 2 – Regeneration efficiency (r_e) for each cycle. C_{in} is the average arsenic concentration of the filtered volume V_{in}, while As_{orig} is the amount of arsenic originally present in the membrane, left over from previous filtration cycles. As_{orig} cannot be directly measured, and is instead calculated from the history of the membrane, by doing a cumulative arsenic mass balance of previous cycles (using records of volume and arsenic concentration of feed, permeate and wash solutions). $C_{j,\text{permeate}}$ represents the arsenic concentration of each permeate aliquot $V_{j,\text{permeate}}$. After each filtration stage, the filter is washed first with 1 M NaOH solution and then with water. $C_{i,\text{wash}}$ represents the arsenic concentration of each wash volume $V_{i,\text{wash}}$ after exiting the filter.

Appendix A.　Supplementary data

Supplementary data associated with this article can be found in the online version at doi:10.1016/j.watres.2010.05.059.

REFERENCES

Attinti, R., Wei, J., Kniel, K., Sims, J.T., Jin, Y., 2010. Virus (MS2, φX174, and Aichi) attachment on sand measured by atomic force microscopy and their transport through sand columns. Environmental Science and Technology 44 (7), 2426–2432.

Bansal, R.C., Goyal, M., 2005. Activated Carbon Adsorption. CRC/Taylor & Francis.

Catalano, J.G., Zhang, Z., Park, C., Fenter, P., Bedzyk, M.J., 2007. Bridging arsenate surface complexes on the hematite (0 1 2) surface. Geochimica et Cosmochimica Acta 71 (8), 1883–1897.

Cortalezzi, M.M., Rose, J., Wells, G., Bottero, J.-Y., Barron, A., Wiesner, M.R., 2003. Ceramic membranes derived from ferroxane nanoparticles: a new route for the fabrication of iron oxide ultrafiltration membranes. Journal of Membrane Science 227 (1–2), 207–217.

Deliyanni, E.A., Bakoyannakis, D.N., Zouboulis, A.I., Matis, K.A., 2003. Sorption of As(V) ions by akaganéite-type nanocrystals. Chemosphere 50 (1), 155–163.

Farquhar, M.L., Charnock, J.M., Livens, F.R., Vaughan, D.J., 2002. Mechanisms of arsenic uptake from aqueous solution by interaction with goethite, lepidocrocite, mackinawite, and

pyrite: an X-ray absorption spectroscopy study. Environmental Science and Technology 36 (8), 1757—1762.

Ferguson, J.G., Davis, J., 1972. A review of the arsenic cycle in natural waters. Water Resources 6, 1259—1274.

Giménez, J., Martínez, M., Pablo, J.d., Rovira, M., Duro, L., 2007. Arsenic sorption onto natural hematite, magnetite, and goethite. Journal of Hazardous Materials 141 (3), 575—580.

Goldberg, S., Johnston, C.T., 2001. Mechanisms of arsenic adsorption on amorphous oxides evaluated using macroscopic measurements, vibrational spectroscopy, and surface complexation modeling. Journal of Colloid and Interface Science 234 (1), 204—216.

Gu, Z., Fang, J., Deng, B., 2005. Preparation and evaluation of GAC-based iron-containing adsorbents for arsenic removal. Environmental Science and Technology 39 (10), 3833—3843.

Hlavay, J., Polyák, K., 2005. Determination of surface properties of iron hydroxide-coated alumina adsorbent prepared for removal of arsenic from drinking water. Journal of Colloid and Interface Science 284 (1), 71—77.

Hódi, M., Polyák, K., Hlavay, J., 1995. Removal of pollutants from drinking water by combined ion exchange and adsorption methods. Environment International 21 (3), 325—331.

Holm, T.R., Anderson, M.A., Iverson, D.G., Standforth, R.S., 1979. Heterogeneous interactions of arsenic in aquatic systems. American Chemical Society Symposium Series 93, 711—736.

Isao, Y., Hiroshi, K., Keihei, U., 1976. Selective adsorption of arsenic ions on silica gel impregnated with ferric hydroxide. Analytical Letters 9 (12), 1125—1133.

Jain, C.K., Ali, I., 2000. Arsenic: occurrence, toxicity and speciation techniques. Water Research 34 (17), 4304—4312.

Jang, M., Shin, E.W., Park, J.K., Choi, S.I., 2003. Mechanisms of arsenate adsorption by highly-ordered nano-structured silicate media impregnated with metal oxides. Environmental Science and Technology 37 (21), 5062—5070.

Kumar, A., Bucciarelli-Tieger, R.H., Gurian, P.L., 2008. Cost-effectiveness of Arsenic Adsorbents. American Water Works Association. Annual Conference and Exposition.

Kundu, S., Gupta, A.K., 2006. Adsorptive removal of As(III) from aqueous solution using iron oxide coated cement (IOCC): evaluation of kinetic, equilibrium and thermodynamic models. Separation and Purification Technology 51 (2), 165—172.

Lakshmipathiraj, P., Narasimhan, B.R.V., Prabhakar, S., Raju, G.B., 2006. Adsorption of arsenate on synthetic goethite from aqueous solutions. Journal of Hazardous Materials 136 (2), 281—287.

Lafferty, B.J., Loeppert, R.H., 2005. Methyl arsenic adsorption and desorption behavior on iron oxides. Environmental Science and Technology 39 (7), 2120—2127.

Lenoble, V., Bouras, O., Deluchat, V., Serpaud, B., Bollinger, J.-C., 2002. Arsenic adsorption onto pillared clays and iron oxides. Journal of Colloid and Interface Science 255 (1), 52—58.

Lenoble, V., Laclautre, C., Deluchat, V., Serpaud, B., Bollinger, J.-C., 2005. Arsenic removal by adsorption on iron(III) phosphate. Journal of Hazardous Materials 123 (1—3), 262—268.

Mandal, B.K., Suzuki, K.T., 2002. Arsenic round the world: a review. Talanta 58, 201—235.

Min, J.H., Hering, J.G., 1998. Arsenate sorption by Fe(III)-doped alginate gels. Water Research 32 (5), 1544—1552.

Mohan, D., Pittman Jr., C.U., 2007. Arsenic removal from water/wastewater using adsorbents — a critical review. Journal of Hazardous Materials 142, 1—53.

Möller, T., Sylvester, P., 2008. Effect of silica and pH on arsenic uptake by resin/iron oxide hybrid media. Water Research 42 (6—7), 1760—1766.

Nicolli, H.B., Suriano, J.M., Peral, M.A.G., Ferpozzi, L.H., Baleani, O. A., 1989. Groundwater contamination with arsenic and other trace-elements in an area of the Pampa province of Cordoba, Argentina. Environmental Geology 14 (1), 3—16.

Pierce, M.L., Moore, C.B., 1982. Adsorption of As(III) and As(V) on amorphous iron hydroxide. Journal of Water Research 16, 1247—1253.

Rau, I., Gonxalo, A., Valiente, M., 2000. Arsenic(V) removal from aqueous solutions by iron(III) loaded chealiting resins. Journal of Radioanalytical and Nuclear Chemistry 246 (3), 597—600.

Raven, K.P., Jain, A., Loeppert, R.H., 1998. Arsenite and arsenate adsorption on ferrihydrite: kinetics, equilibrium, and adsorption envelopes. Environmental Science and Technology 32 (3), 344—349.

Reed, B.E., Vaughan, R., Jiang, L., 2000. As(III), As(V), Hg, and Pb removal by Fe-oxide impregnated activated carbon. Journal of Environmental Engineering 126, 869.

Rose, J., Cortalezzi-Fidalgo, M., Moustier, S., Magnetto, C., Jones, C., Barron, A., Wiesner, M., Bottero, J.-Y., 2002. Synthesis and characterization of carboxylate-FeOOH nanoparticles (ferroxanes) and ferroxane-derived ceramics. Chemistry of Materials 14, 621—628.

Schwertmann, U., Cornell, R.M., 1991. Iron Oxides in the Laboratory. Preparation and Characterisation. VCH, New York.

Schwertmann, U., Cornell, R.M., 2000. The Iron Oxides. Structure, Properties, Reactions Occurrences and Uses. VCH, Weinheim.

Shigetomi, Y., Hori, Y., Kojima, T., 1980. The removal of arsenate in waste water with an adsorbent prepared by binding hydrous iron(III) oxide with polyacrylamide. Bulletin of the Chemical Society of Japan 53, 1475—1476.

Singh, D.B., Prasad, G., Rupainwar, D.C., 1996. Adsorption technique for the treatment of As(V)-rich effluents. Colloids and Surfaces A: Physicochemical and Engineering Aspects 111 (1—2), 49—56.

Smedley, P.L., Kinniburg, D.G., 2005. Sources and behaviour of arsenic in natural water. Chapter 1 in United Nations Synthesis Report on Arsenic in Drinking Water.

Smith, A.H., Lingas, E.O., Rahman, M., 2000. Contamination of drinking-water by arsenic in Bangladesh: a public health emergency. Bulletin of the World Health Organization 78 (9), 1093—1103.

Solozhenkin, P.M., Deliyanni, E.A., Bakoyannakis, V.N., Zouboulis, A.I., Matis, K.A., 2003. Removal of As(V) ions from solution by akaganeite bgr-FeO(OH) nanocrystals. Journal of Mining Science 39 (3), 287—296.

Thirunavukkarasu, O.S., Viraghavan, T., Subramanian, K.S., 2003. Arsenic removal from drinking water using iron oxide coated sand. Water, Air, and Soil Pollution 142, 95—111.

Vaishya, R.C., Gupta, S.K., 2004. Modeling arsenic(III) adsorption from water by sulfate modified iron-oxide coated sand (SMIOCS). Separation Science and Technology 39 (3), 645—666.

WHO, 2007. Fact Sheet No 210: Arsenic in Drinking Water. Revised May 2001. http://www.who.int/mediacentre/factsheets/fs210/en/index.html.

Xu, H., Allard, B., Grimvall, A., 1988. Influence of pH and organic substance on the adsorption of As(V) on geologic materials. Water, Air, and Soil Pollution 40 (3—4), 293—305.

Yoshitake, H., Yokoi, T., Tatsumi, T., 2003. Adsorption behavior of arsenate at transition metal cations captured by amino-functionalized mesoporous silicas. Chemistry of Materials 15 (8), 1713—1721.

Zhang, Y., Yang, M., Huang, Xia, 2003. Arsenic(V) removal with a Ce(IV)-doped iron oxide adsorbent. Chemosphere 51 (9), 945—952.

Zouboulis, A.I., Katsoyiannis, I.A., 2002. Arsenic removal using iron oxide loaded alginate beads. Industrial & Engineering Chemistry Research 42 (24), 6149—6155.